Available online at www.sciencedirect.com
SCIENCE DIRECT
Journal of Organometallic Chemistry 691 (2006) 3771–3781
Journal of Organometallic Chemistry
www.elsevier.com/locate/jorganchem

Regiospecific and sequential P–C bond activation/cluster transformations in the reaction of $PhCCo_2MoCp(CO)_8$ with the diphosphine ligands 2,3-bis(diphenylphosphino)maleic anhydride (bma) and 3,4-bis(diphenylphosphino)-5-methoxy-2(5H)-furanone (bmf)

Simon G. Bott [a,*], Kaiyuan Yang [b], Michael G. Richmond [b,*]

[a] Department of Chemistry, University of Houston, Houston, TX 77004, USA
[b] Department of Chemistry, University of North Texas, P.O. Box 305070, Denton, TX 76203-5070, USA

Received 26 January 2006; received in revised form 16 May 2006; accepted 16 May 2006
Available online 25 May 2006

Abstract

Thermolysis of the mixed-metal cluster $PhCCo_2MoCp(CO)_8$ (**1**) with the diphosphine ligand 2,3-bis(diphenylphosphino)maleic anhydride (bma) in CH_2Cl_2 leads to the sequential formation of the phosphido-bridged cluster $Co_2MoCp(CO)_5[\mu_2,\eta^2,\eta^1$-C(Ph)C=C(PPh$_2$)C(O)OC(O)$](\mu$-PPh$_2$) (**3**) and the bis(phosphido)-bridged cluster $Co_2MoCp(CO)_4[\eta^3,\eta^1,\eta^1$-C(Ph)C=CC(O)O-C(O)$](\mu$-PPh$_2)_2$ (**4**). **3** and **4** have been isolated and characterized in solution by IR and NMR (^{1}H, ^{13}C, and ^{31}P) spectroscopies, and the solid-state structures have been established by X-ray diffraction analyses. Both clusters contain 48e- and exhibit triangular Co_2Mo cores. The structure of **3** reveals the presence of a phosphido moiety that bridges the Co–Co vector and a six-electron μ_2,η^2,η^1-C(Ph)C=C(PPh$_2$)C(O)OC(O) ligand that caps one of the Co_2Mo faces. The X-ray structure of **4** confirms that the five-electron η^3,η^1,η^1-C(Ph)C=CC(O)OC(O) ligand is σ-bound to the two cobalt centers in an η^1 fashion and π-coordinated to the molybdenum center through a traditional η^3-allylic interaction. The reaction between $PhCCo_2MoCp(CO)_8$ and the chiral diphosphine ligand 3,4-bis(diphenylphosphino)-5-methoxy-2(5H)-furanone (bmf) proceeds similarly, furnishing the phosphido-bridged cluster $Co_2MoCp(CO)_5$ $[\mu_2,\eta^2,\eta^1$-C(Ph)C=C(PPh$_2$)C(O)OCH(OMe)$](\mu$-PPh$_2$) (**6**), followed by conversion to $Co_2MoCp(CO)_4[\eta^3,\eta^1,\eta^1$-C(Ph)C=CC(O)O-CH(OMe)$](\mu$-PPh$_2)_2$ (**7**). The identities of clusters **6** and **7** have been ascertained by solution spectroscopic methods and X-ray crystallography. The overall molecular structure of cluster **6** is similar to that of cluster **3**, except that the P–C(furanone ring) bond cleavage occurs with high regioselectivity and high diastereoselectivity. The cleavage of the remaining P–C(furanone ring) bond in cluster **6** gives rise to the bis(phosphido)-bridged cluster **7**, whose structure is discussed relative to its bma-derived analogue **4**. The diastereoselectivity that accompanies the formation of **6** and **7** is discussed relative to steric effects within the Co_2Mo polyhedron. The cyclic voltammetric properties of cluster **3** have been examined, with three well-defined one-electron processes for the 0/+1, 0/−1, −1/−2 redox couples found. The composition of the HOMO and LUMO in **3** was established by extended Hückel MO calculations, with the data discussed relative to the parent tetrahedrane cluster **1**.

Keywords: Mixed-metal clusters; Ligand substitution; P–C bond cleavage; Chiral clusters

1. Introduction

The reaction of the diphosphine ligands 2,3-bis(diphenylphosphino)maleic anhydride (bma) and 3,4-bis(diphenylphosphino)-5-methoxy-2(5H)-furanone (bmf) with the tetrahedrane clusters $RCCo_3(CO)_9$ (R = Ph, Fc) and

* Corresponding authors. Tel.: +1 713 743 2771 (S.G. Bott); Tel.: +1 940 565 3548 (M.G. Richmond).
E-mail addresses: sbott@uh.edu (S.G. Bott), cobalt@unt.edu (M.G. Richmond).

0022-328X/$ - see front matter © 2006 Elsevier B.V. All rights reserved.
doi:10.1016/j.jorganchem.2006.05.027

$RCCo_2NiCp(CO)_6$ (R = Ph, H) has been actively investigated by our groups the last several years [1–4]. The structures of these rigid diphosphine ligands are shown to the right. Coordination of the these diphosphine ligands at each type of cluster affords the corresponding substituted products $RCCo_3(CO)_7$(P–P) and $RCCo_2NiCp(CO)_4$(P–P). The electron-withdrawing carbonyl groups on the maleic anhydride (bma) and furanone (bmf) rings promote the degradation of the $RCCo_3(CO)_7$(P–P) and $RCCo_2NiCp(CO)_4$(P–P) clusters, with the oxidative cleavage of one P–C ligand bond serving as a point of entry for the observed diphosphine/cluster activation. The course and outcome of these reactions depend on several variables, one of which is the metallic composition of the cluster, as shown in Scheme 1 for the phenyl-capped clusters $PhCCo_3(CO)_7$(bma) and $PhCCo_2NiCp(CO)_4$(bma). Thermolysis of the bma-substituted Co_3 and Co_2Ni clusters furnishes the structurally different phosphido-bridged clusters $Co_3(CO)_6[\mu_2,\eta^2,\eta^1$-C(Ph)C=C($PPh_2$)C(O)OC(O)]($\mu$-$PPh_2$) and $Co_2NiCp(CO)_4[\mu_2,\eta^2,\eta^1$-C(Ph)C=C($PPh_2$)C(O)OC(O)]($\mu$-$PPh_2$). Both phosphido-bridged clusters are thermally sensitive; the former homometallic cluster undergoes gross decomposition when heated at temperatures >80 °C while the latter Co_2Ni cluster furnishes the mononuclear nickel compound CpNi[PPh_2CPhC=C(PPh_2)C(O)OC(O)]. Definitive proof for the enhanced diphosphine ligand reactivity in $PhCCo_3(CO)_7$(bma) and $PhCCo_2NiCp(CO)_4$(bma) derives from the synthesis of the related clusters containing the archetypal diphosphine ligand (*Z*)-Ph_2PCH=$CHPPh_2$. The structurally similar $PhCCo_3(CO)_7$[(*Z*)-Ph_2PCH=$CHPPh_2$] [5] and $PhCCo_2NiCp(CO)_4$[(*Z*)-Ph_2PCH=$CHPPh_2$] [6] clusters have been shown to be stable under conditions comparable to those used to promote the transformations illustrated in Scheme 1.

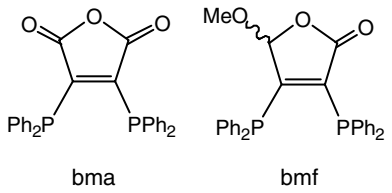

The synthesis and reactivity of the chiral clusters $HCCo_2NiCp(CO)_4$(bmf) and $PhCCo_2NiCp(CO)_4$(bmf) have recently been described by us [4]. Both bmf-substituted clusters exist as a ca. 70:30 mixture of diastereomers in solution and are obtained in good yield from thermolysis of the $RCCo_2NiCp(CO)_6$ in the presence of added bmf ligand. Here the bridging bmf ligand is equatorially disposed across the Co–Co bond in each product, as deduced by NMR analyses. The important role played by the capping R-group in controlling the chemistry exhibited by these bmf-substituted clusters was verified during routine thermolysis studies of $HCCo_2NiCp(CO)_4$(bmf) and $PhCCo_2NiCp(CO)_4$(bmf). Whereas heating $PhCCo_2NiCp(CO)_4$(bmf) at 83 °C leads to cluster decomposition, the latter methylidyne cluster undergoes a regiospecific cleavage of one of the two distinct P–C(furanone) bonds, followed by diastereoselective formation of the phosphido-bridged cluster $Co_2NiCp(CO)_4[\mu_2,\eta^2,\eta^1$-C(H)C=C($PPh_2$)C(O)O-CH(OMe)]($\mu$-$PPh_2$). This transformation is depicted in Eq. (1). Of interest to us was the oxidative P–C bond cleavage of the least basic phosphine moiety at the C-4 atom of the furanone ring [7]. The release or slippage of one of the phosphine moieties from a bidentate coordinated bmf ligand is believed to promote the observed P–C bond cleavage at the cluster. The selective dissociation of the less strongly bound phosphine moiety, followed by its subse-

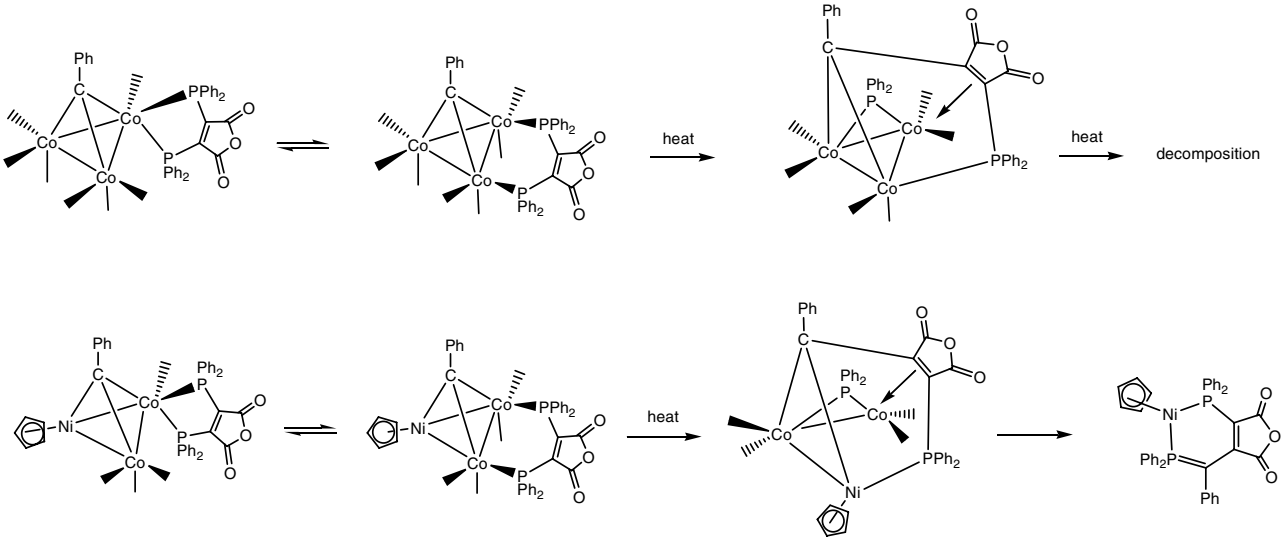

Scheme 1.

quent activation, provides crucial insight into the degradation pathway that such a chiral auxiliary might experience during asymmetric catalysis.

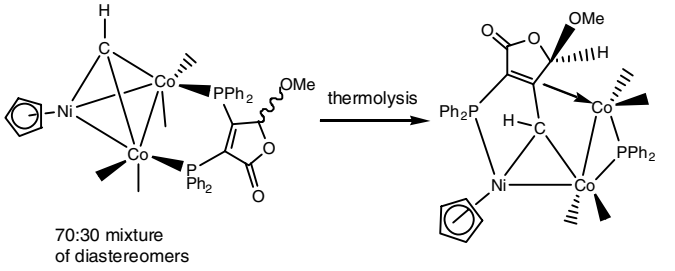

(1)

Herein we present our data on the ligand substitution in the mixed-metal tetrahedrane cluster $PhCCo_2MoCp(CO)_8$ with the diphosphine ligands bma and bmf. To our knowledge, the ligand substitution chemistry of this cluster with bidentate phosphines has received scant attention [8], with our report on $PhCCo_2MoCp(CO)_6[(Z)\text{-}Ph_2PCH{=}CHPPh_2]$ representing the only structurally characterized derivative of **1** that possesses a bidentate ligand [6]. Thermolysis of $PhCCo_2MoCp(CO)_8$ with bma leads to the rapid replacement of multiple CO groups and diphosphine coordination to furnish the phosphido-bridged clusters $Co_2MoCp(CO)_5[\mu_2,\eta^2,\eta^1\text{-}C(Ph)C{=}C(PPh_2)C(O)OC(O)](\mu\text{-}PPh_2)$ (**3**) and $Co_2MoCp(CO)_4[\eta^3,\eta^1,\eta^1\text{-}C(Ph)C{=}CC(O)OC(O)](\mu\text{-}PPh_2)_2$ (**4**). The reaction of **1** with added bmf proceeds similarly and with a high degree of regio- and diastereoselectivity to give $Co_2MoCp(CO)_5[\mu_2,\eta^2,\eta^1\text{-}C(Ph)C{=}C(PPh_2)C(O)OCH(OMe)](\mu\text{-}PPh_2)$ (**6**) and $Co_2MoCp(CO)_4[\eta^3,\eta^1,\eta^1\text{-}C(Ph)C{=}CC(O)OCH(OMe)](\mu\text{-}PPh_2)_2$ (**7**). The solution spectroscopic data and the X-ray diffraction structures of clusters **3**, **4**, **6**, and **7** confirm the identities of the substitution products and allow for the delineation of a working reaction sequence. The regio- and diastereoselectivity that accompany the cleavage of the PPh_2 moiety associated with the bmf ligand and the subsequent coupling of the furanone ring with the μ_3-benzylidyne capping ligand in cluster **6** is discussed with respect to related chemistry from our labs. The subtle but important electronic perturbation exerted on the two PPh_2 moieties in the bmf ligand by the furanone ring is discussed in the context of the observed P–C bond cleavage reactivity.

2. Experimental

2.1. General methods

The mixed-metal cluster $PhCCo_2MoCp(CO)_8$ was synthesized according to the procedure of Vahrenkamp, using $PhCCo_3(CO)_9$ and $Cp_2Mo_2(CO)_6$ [9]. The diphosphine ligands bma and bmf were prepared from 2,3-dichloromaleic anhydride and 3,4-dichloro-5-hydroxy-2(5H)-furanone and Ph_2PSiMe_3 and Ph_2PK, respectively [10,11]. The ^{13}CO (>99%) used in the enrichment of $PhCCo_2MoCp(CO)_8$ was purchased from Isotec, Inc. All reaction and NMR solvents were distilled under argon from a suitable drying agent and stored in Schlenk storage vessels [12]. The tetra-*n*-butylammonium perchlorate (TBAP) that was used as an electrolyte in the cyclic voltammetry studies was purchased from Johnson Matthey Electronics and recrystallized from ethyl acetate/hexane. The recrystallized TBAP was dried under high vacuum for at least 36 h prior to use. The combustion analyses were performed by Atlantic Microlab, Norcross, GA.

The reported infrared data were recorded on a Nicolet 20 SXB FT-IR spectrometer in 0.1 mm amalgamated NaCl cells, using PC control and OMNIC software, while the ^1H (300 MHz), ^{13}C (75 MHz), and ^{31}P NMR (121 MHz) spectra were recorded on a Varian 300-VXR spectrometer. All reported ^{13}C and ^{31}P NMR data were acquired in the proton-decoupled mode.

2.2. Thermolysis of $PhCCo_2MoCp(CO)_8$ with bma

To a large Schlenk vessel under argon flush was charged 0.40 g (0.68 mmol) of $PhCCo_2MoCp(CO)_8$ and 0.38 g (0.82 mmol) of bma, after which 50 mL of CH_2Cl_2 was added by syringe. The reaction was heated at reflux overnight under argon and examined by TLC analysis using a 3:1 mixture of CH_2Cl_2/petroleum ether as the eluent. Two major bands were observed that were subsequently shown to be cluster **3** (green; $R_f = 0.60$) and cluster **4** (brown, $R_f = 0.50$), in addition to a substantial amount(s) of decomposed material(s) that remained at the origin of the TLC plate. Clusters **3** and **4** were isolated by column chromatography over silica gel using the aforementioned solution system. Cluster **3** was recrystallized from CH_2Cl_2/Et_2O to afford the combustion sample and single crystals of **3** suitable for X-ray diffraction analysis. Cluster **4** was recrystallized from CH_2Cl_2 and hexane, which afforded X-ray quality crystals and the analytical sample. Yield of **3**: 0.25 g (38%). IR (CH_2Cl_2): ν(CO) 2052 (s), 2034 (vs), 2016 (m), 1998 (m), 1800 (b, m, bridging CO and sym bma C=O), 1743 (m, antisym bma C=O) cm^{-1}. ^1H NMR (C_6D_6): δ 5.05 (s, Cp), 6.44–8.53 (m, phenyl groups). ^{13}C NMR (CH_2Cl_2; 183 K): δ 193.45 (s, Co–CO), 195.27 (s, Co–CO), 201.81 (s, Co–CO), 202.82 (s, Co–CO), 241.52 (s, bridging CO). ^{31}P NMR (CH_2Cl_2; 183 K): δ 21.29 (phosphine), 179.59 (phosphido). Anal. Calc. (found) for $C_{45}H_{30}Co_2MoO_8P_2 \cdot 1/2Et_2O$: C, 55.81 (55.40); H, 3.50 (3.51). Yield of **4**: 0.20 g (30%). IR (CH_2Cl_2): ν(CO) 2056 (vs), 2024 (m), 1948 (s), 1815 (m, sym bma C=O), 1785 (s, bridging CO), 1756 (m, antisym bma C=O) cm^{-1}. ^1H NMR (C_6D_6): δ 5.15 (s, Cp), 6.30–7.90 (m, phenyl groups). ^{13}C NMR (CH_2Cl_2; 183 K): δ 191.73 (s, Co–CO), 200.51 (s, Co–CO), 207.94 (s, Co–CO), 250.52 (s, bridging CO). ^{31}P NMR (CH_2Cl_2; 183 K): δ 209.04 (d, phosphido, $J_{P-P} = 48$ Hz), 251.93 (d, phosphido, $J_{P-P} = 48$ Hz). Anal. Calc. (found) for $C_{44}H_{30}Co_2MoO_7P_2$: C, 55.79 (55.98); H, 3.17 (3.67).

2.3. Thermolysis of $PhCCo_2MoCp(CO)_8$ with bmf

The reaction between $PhCCo_2MoCp(CO)_8$ and bmf was carried similarly as that described above using bma. Here

0.13 g (0.22 mmol) of $PhCCo_2MoCp(CO)_8$ and 0.13 g (0.26 mmol) of bmf were heated over night in CH_2Cl_2. TLC examination of the cooled reaction solution using a 1:1 mixture of CH_2Cl_2/petroleum ether as the eluent showed the presence of some unreacted $PhCCo_2MoCp(CO)_8$, green and brown spots for clusters **6** ($R_f = 0.55$) and **7** ($R_f = 0.30$), respectively, and decomposed material at the origin of the plate. The two products were isolated by column chromatography over silica gel using CH_2Cl_2/petroleum ether (1:1). Both clusters were recrystallized from CH_2Cl_2/hexane to furnish the crystals used in the X-ray diffraction studies and the combustion analyses. Yield of **6**: 55 mg (25%). IR (CH_2Cl_2): ν(CO) 2046 (s), 2027 (vs), 2007 (m), 1974 (b, m), 1781 (b, m, bridging CO), 1734 (m, bmf C═O) cm^{-1}. ^1H NMR (C_6D_6): δ 2.81 (s, MeO), 4.96 (s, Cp), 5.68 (s, methine), 6.75–8.15 (m, phenyl groups). ^{13}C NMR (CH_2Cl_2; 183 K): δ 194.39 (s, Co–CO), 196.07 (s, Co–CO), 202.18 (s, Co–CO), 203.54 (s, Co–CO), 244.06 (s, bridging CO). ^{31}P NMR (CH_2Cl_2; 183 K): δ 22.94 (phosphine), 179.29 (phosphido). Anal. Calc. (found) for $C_{46}H_{34}Co_2MoO_8P_2 \cdot 1/4CH_2Cl_2$: C, 54.60 (54.67); H, 3.75 (4.03). Yield of **7**: 55 mg (26%). IR (CH_2Cl_2): ν(CO) 2050 (vs), 2014 (s), 1937 (s), 1779 (s, bridging CO), 1736 (m, bmf C═O) cm^{-1}. ^1H NMR (C_6D_6): δ 2.66 (s, MeO), 4.71 (s, Cp), 5.82 (s, methine), 6.84–8.15 (m, phenyl groups). ^{13}C NMR (CH_2Cl_2; 183 K): δ 192.44 (s, Co–CO), 201.67 (s, Co–CO), 209.17 (s, Co–CO), 255.03 (s, bridging CO). ^{31}P NMR (CH_2Cl_2; 183 K): δ 213.33 (b, phosphido), 251.54 (d, phosphido). Anal. Calc. (found) for $C_{45}H_{34}Co_2MoO_7P_2 \cdot CH_2Cl_2$: C, 52.53 (52.83); H, 3.75 (3.87).

2.4. X-ray structural determinations

Tables 1 and 2 contain the X-ray data and processing parameters and selected bond distances and angles, respectively, for clusters **3**, **4**, **6**, and **7**. A suitable X-ray quality crystal of each cluster was grown, as described above, and sealed inside a Lindemann capillary, followed by mounting on an Enraf-Nonius CAD-4 diffractometer. After the cell constants were obtained, intensity data in the range of $2° \leqslant 2\theta \leqslant 40°$ (**3** and **6**) and $2° \leqslant 2\theta \leqslant 44°$ (**5** and **7**) were collected at 298 K and were corrected for Lorentz, polarization, and absorption (DIFABS). The structures of clusters **3**, **4**, and **6** were solved from the Patterson, which revealed the positions of the Mo, Co, and P atoms. Cluster **7** was solved by using Multan. All non-hydrogen atoms were located with difference Fourier maps and full-matrix least-squares refinement. Due to the poor scattering displayed by the crystal of **3**, only the Mo, Co, and P atoms were refined anisotropically. In the case of **6**, all non-hydrogen atoms were refined anisotropically, with the exception of the carbon and chlorine atoms. Refinement of clusters **4** and **7** followed similar data reduction procedures, with all phenyl carbon atoms and the carbon and chlorine atoms of the solvent molecule (for **7**) refined isotropically. All hydrogen atoms were assigned calculated positions and allowed to ride on the attached heavy atom. Refinement on **3** converged at $R = 0.0733$ and $R_w = 0.0896$ for 1758 unique reflections with $I > 2.5\sigma(I)$, while **4** afforded convergence values of $R = 0.0780$ and $R_w = 0.1006$ for 2729 unique reflections with $I > 3\sigma(I)$. The refinement of **6** and **7** converged at $R = 0.0572$ and

Table 1
X-ray crystallographic data and processing parameters for the Co_2Mo clusters **3**, **4**, **6**, and **7**

Compound number	**3**	**4**	**6**	**7**
CCDC entry no.	276391	276392	274194	274193
Mol. formula	$C_{45}H_{30}Co_2MoO_8P_2 \cdot 1/2Et_2O$	$C_{44}H_{30}Co_2MoO_7P_2$	$C_{47}H_{34}Co_2MoO_8P_2 \cdot CH_2Cl_2$	$C_{45}H_{34}Co_2MoO_7P_2 \cdot 1/2CH_2Cl_2$
Formula weight	1011.55	946.48	1074.46	1004.99
Space group	Triclinic, $P\bar{1}$	Triclinic, $P\bar{1}$	Monoclinic, $P2_1/n$	Triclinic, $P\bar{1}$
a (Å)	10.205(1)	11.580(2)	11.949(2)	10.505(1)
b (Å)	10.344(1)	12.957(2)	20.803(3)	11.176(1)
c (Å)	20.265(3)	16.310(2)	18.804(2)	19.500(2)
α (°)	85.542(1)	101.06(1)		95.902(8)
β (°)	78.50(1)	106.03(1)	107.07(1)	92.383(8)
γ (°)	87.81(1)	95.38(1)		112.732(8)
V (Å^3)	2089(1)	2280.2(6)	4468(1)	2092.1(4)
Formula units per cell (Z)	2	2	4	2
D_{calcd} (g/cm^3)	1.608	1.378	1.597	1.595
λ (Mo Kα) (Å)	0.71073	0.71073	0.71073	0.71073
Absorption coeff. (cm^{-1})	12.02	10.94	12.46	12.60
Max/min trans.	0.84/1.12	0.85/1.03	0.76/1.36	0.87/1.13
Total reflections	3907	5583	5970	5123
Independent reflections	1758	2729	2631	3202
Data/res/parameters	1758/0/270	2729/0/345	2631/0/314	3202/0/402
R	0.0733	0.0780	0.0572	0.0577
R_w	0.0896	0.1006	0.0648	0.0796
GOF on F^2	0.99	1.23	0.98	2.10
weights	$[0.04F^2 + (\sigma F)^2]^{-1}$	$[0.04F^2 + (\sigma F)^2]^{-1}$	$[0.04F^2 + (\sigma F)^2]^{-1}$	$[0.04F^2 + (\sigma F)^2]^{-1}$
Largest difference in peak and hole (e/Å^3)	0.92, −0.92	1.34, −0.95	0.76, −0.71	1.05, −0.88

Table 2
Selected bond distances (Å) and angles (°) for the Co_2Mo clusters **3**, **4**, **6**, and **7**[a]

*Cluster **3***			
Bond distances			
Mo–Co(1)	2.699(5)	Mo–Co(2)	2.929(4)
Mo–P(2)	2.354(8)	Mo–Cp(centroid)	2.01(1)
Mo–C(1)	1.87(3)	Mo–C(16)	2.12(2)
Co(1)–Co(2)	2.643(6)	Co(1)–P(1)	2.262(7)
Co(1)–C(1)	2.45(3)	Co(1)–C(2)	1.65(3)
Co(1)–C(3)	1.67(3)	Co(1)–C(16)	2.05(2)
Co(2)–P(2)	2.272(7)	Co(2)–C(4)	1.69(3)
Co(2)–C(5)	1.72(3)	Co(2)–C(11)	2.04(3)
Co(2)–C(15)	2.10(2)	C(11)–C(15)	1.38(3)
C(15)–C(16)	1.56(4)		
Bond angles			
Co(1)–Mo–Co(2)	55.8(1)	Mo–Co(1)–Co(2)	66.5(1)
Mo–Co(2)–Co(1)	57.7(1)	P(1)–Co(1)–C(16)	85.6(7)
P(2)–Co(2)–C(11)	151.0(8)	P(2)–Co(2)–C(15)	112.6(7)
C(11)–Co(2)–C(15)	39(1)	Co(1)–P(1)–C(11)	88.9(8)
Mo–P(2)–Co(2)	78.5(3)	Mo–C(16)–Co(1)	80.5(8)
Mo–C(1)–O(1)	168(2)	Co(1)–C(1)–O(1)	113(2)
P(2)–Mo–C(1)	93.0(9)	P(2)–Mo–C(16)	118.7(7)
*Cluster **4***			
Bond distances			
Mo–Co(1)	2.627(3)	Mo–Co(2)	2.748(3)
Mo–P(1)	2.453(6)	Mo-Cp(centroid)	2.01(1)
Mo–C(11)	2.22(2)	Mo–C(15)	2.31(2)
Mo–C(16)	2.44(2)	Mo–C(1)	1.98(2)
Co(1)–Co(2)	2.666(5)	Co(1)–P(1)	2.168(7)
Co(1)–P(1)	2.131(7)	Co(1)–C(2)	1.71(2)
Co(1)–C(16)	1.92(2)	Co(2)–P(2)	2.233(7)
Co(2)–C(1)	2.12(2)	Co(2)–C(3)	1.72(3)
Co(2)–C(4)	1.79(2)	Co(2)–C(11)	1.93(2)
C(11)–C(15)	1.46(3)	C(15)–C(16)	1.34(3)
Bond angles			
Co(1)–Mo–Co(2)	59.4(1)	Mo–Co(1)–Co(2)	62.5(1)
Mo–Co(2)–Co(1)	58.04(9)	Co(2)–Mo–P(1)	80.6(2)
P(1)–Mo–C(1)	85.8(6)	P(1)–Mo–C(11)	120.5(5)
P(1)–Mo–C(15)	119.5(5)	P(1)–Mo–C(16)	90.5(4)
C(1)–Mo–C(11)	74.7(8)	C(1)–Mo–C(15)	112.1(9)
C(1)–Mo–C(16)	128.5(8)	C(11)–Mo–C(15)	37.4(8)
C(11)–Mo–C(16)	63.4(8)	C(15)–Mo–C(16)	32.6(8)
P(1)–Co(1)–P(2)	132.1(3)	P(1)–Co(1)–C(16)	116.4(6)
P(2)–Co(1)–C(16)	94.0(7)	P(2)–Co(2)–C(11)	95.2(6)
C(1)–Co(2)–C(11)	78.2(8)	Mo–P(1)–Co(1)	69.0(2)
Co(1)–P(2)–Co(2)	75.3(2)	Mo–C(1)–O(1)	156(1)
Co(2)–C(1)–O(1)	119(1)	Mo–C(15)–C(11)	68(1)
Mo–C(15)–C(16)	79(1)	C(11)–C(15)–C(16)	123(2)
Co(1)–C(16)–C(15)	119(2)		
*Cluster **6***			
Bond distances			
Mo–Co(1)	2.681(2)	Mo–Co(2)	2.915(2)
Mo–P(2)	2.358(4)	Mo-Cp(centroid)	2.00(1)
Mo–C(1)	1.91(1)	Mo–C(16)	2.10(2)
Co(1)–Co(2)	2.635(3)	Co(1)–P(1)	2.226(4)
Co(1)–C(1)	2.38(2)	Co(1)–C(2)	1.79(1)
Co(1)–C(3)	1.81(1)	Co(1)–C(16)	2.04(1)
Co(2)–P(2)	2.261(5)	Co(2)–C(4)	1.77(1)
Co(2)–C(5)	1.75(1)	Co(2)–C(11)	2.04(1)
Co(2)–C(15)	2.12(1)	C(11)–C(15)	1.45(2)
C(15)–C(16)	1.49(2)		

Table 2 (*continued*)

Bond angles			
Co(1)–Mo–Co(2)	55.99(6)	Mo–Co(1)–Co(2)	66.50(6)
Mo–Co(2)–Co(1)	57.51(6)	P(1)–Co(1)–C(16)	85.0(4)
P(2)–Co(2)–C(11)	153.8(4)	P(2)–Co(2)–C(15)	114.5(4)
C(11)–Co(2)–C(15)	40.7(5)	Co(1)–P(1)–C(11)	90.7(5)
Mo–P(2)–Co(2)	78.2(1)	Mo–C(16)–Co(1)	80.6(5)
Mo–C(1)–O(1)	164(1)	Co(1)–C(1)–O(1)	119.4(9)
P(2)–Mo–C(1)	89.8(5)	P(2)–Mo–C(16)	116.7(4)
O(14)–C(14)–C(15)	111(1)	O(13)–C(14)–O(14)	108(1)
*Cluster **7***			
Bond distances			
Mo–Co(1)	2.620(2)	Mo–Co(2)	2.751(2)
Mo–P(1)	2.459(3)	Mo–Cp(centroid)	1.99(1)
Mo–C(11)	2.25(1)	Mo–C(15)	2.36(1)
Mo–C(16)	2.36(1)	Mo–C(4)	2.06(1)
Co(1)–Co(2)	2.659(2)	Co(1)–P(1)	2.173(3)
Co(1)–P(2)	2.132(3)	Co(1)–C(1)	1.75(1)
Co(1)–C(16)	1.91(1)	Co(2)–P(2)	2.244(3)
Co(2)–C(2)	1.77(1)	Co(2)–C(3)	1.76(1)
Co(2)–C(4)	2.075(9)	Co(2)–C(11)	1.92(1)
C(11)–C(15)	1.43(2)	C(15)–C(16)	1.42(2)
Bond angles			
Co(1)–Mo–Co(2)	59.29(5)	Mo–Co(1)–Co(2)	62.80(5)
Mo–Co(2)–Co(1)	57.91(5)	Co(2)–Mo–P(1)	79.59(8)
P(1)–Mo–C(4)	87.7(3)	P(1)–Mo–C(11)	119.9(3)
P(1)–Mo–C(15)	122.0(3)	P(1)–Mo–C(16)	91.4(3)
C(4)–Mo–C(11)	70.3(4)	C(4)–Mo–C(15)	106.5(4)
C(4)–Mo–C(16)	126.5(4)	C(11)–Mo–C(15)	36.2(4)
C(11)–Mo–C(16)	64.2(4)	C(15)–Mo–C(16)	35.1(4)
P(1)–Co(1)–P(2)	131.9(2)	P(1)–Co(1)–C(16)	115.3(3)
P(2)–Co(1)–C(16)	94.0(3)	P(2)–Co(2)–C(11)	94.8(3)
C(4)–Co(2)–C(11)	77.1(4)	Mo–P(1)–Co(1)	68.6(1)
Co(1)–P(2)–Co(2)	74.78(9)	Mo–C(4)–Co(2)	83.3(4)
Mo–C(4)–O(4)	150.0(8)	Co(2)–C(4)–O(4)	126.5(9)
Mo–C(15)–C(11)	68.0(6)	Mo–C(15)–C(16)	72.6(6)
C(11)–C(15)–C(16)	118(1)	Co(1)–C(16)–C(15)	121.2(9)

[a] Numbers in parentheses are estimated standard deviations in the least

$R_w = 0.0648$ for 2631 unique reflections with $I > 3\sigma(I)$ and $R = 0.0577$ and $R_w = 0.0796$ for 3202 unique reflections with $I > 3\sigma(I)$, respectively.

2.5. Extended Hückel MO data for $Co_2MoCp(CO)_5[\mu_2,\eta^2,\eta^1\text{-}C(H)C{=}C(PH_2)C(O)OC(O)](\mu\text{-}PH_2)$

The extended Hückel calculations on the phosphido-bridged cluster $Co_2MoCp(CO)_5[\mu_2,\eta^2,\eta^1\text{-}C(Ph_2)C{=}C(PPh_2)C(O)OC(O)](\mu\text{-}PPh_2)$ (**3**) were carried out with the original program developed by Hoffmann and Libscomb [13], as modified by Mealli and Proserpio [14], using the weighted H_{ij}'s contained in the program. The input Z-matrix for the model cluster $Co_2MoCp(CO)_5[\mu_2,\eta^2,\eta^1\text{-}C(H)C{=}C(PH_2)C(O)OC(O)](\mu\text{-}PH_2)$ was constructed using the X-ray fractional coordinates from **3**. All phenyl groups were replaced by a hydrogen atom, with the carbene C–H and P–H bond lengths assigned distances of 1.03 and 1.41 Å, respectively [15].

2.6. Cyclic voltammetry

The cyclic voltammetric data were recorded on a PAR Model 273 potential/galvanostat, employing positive feedback circuitry to compensate of *i*R drop. The airtight CV cell used was based on a standard three-electrode design, with two platinum disks serving as the working and auxiliary electrodes. A silver wire was used as a quasi-reference electrode, and the reported potential data are referenced to the formal potential of internally added Cp^*_2Fe, whose oxidation potential was taken as $E_{1/2} = -0.23$ V [16].

3. Results and discussion

3.1. Synthesis, spectroscopic data, and X-ray diffractions structures for $Co_2MoCp(CO)_5[\mu_2,\eta^2,\eta^1$-$C(Ph)C{=}C(PPh_2)C(O)OC(O)](\mu$-$PPh_2)$ (3) and $Co_2MoCp(CO)_4[\eta^3,\eta^1,\eta^1$-$C(Ph)C{=}CC(O)OC(O)](\mu$-$PPh_2)_2$ (4)

The reaction of $PhCCo_2MoCp(CO)_8$ with a slight excess of bma (1.2 eq.) in refluxing CH_2Cl_2 furnishes the new cluster compounds $Co_2MoCp(CO)_5[\mu_2,\eta^2,\eta^1$-C(Ph)C=C(PPh$_2$)C(O)OC(O)](μ-PPh$_2$) (**3**) and $Co_2MoCp(CO)_4$-$[\eta^3,\eta^1,\eta^1$-C(Ph)C=CC(O)OC(O)](μ-PPh$_2$)$_2$ (**4**) in 30–40% yields. The two cluster products were subsequently isolated by column chromatography over silica gel and characterized in solution by IR and NMR spectroscopies. The replacement of two CO groups by the bma ligand is expected to give the simple substitution product $PhCCo_2$-$MoCp(CO)_6$(bma), which is not stable under the reaction conditions. Indirect proof of this assertion derives from the substitution of cluster **1** with the unsaturated diphosphine ligand (*Z*)-$Ph_2PCH{=}CHPPh_2$. Here the replacement of two CO groups yields the ligand-bridged cluster $PhCCo_2MoCp(CO)_6[(Z)$-$Ph_2PCH{=}CHPPh_2]$, which serves as a structural analog for $PhCCo_2MoCp(CO)_6$(bma), is stable under the conditions employed in above thermolysis [6]. The greater reactivity of a cluster-coordinated bma ligand vis-á-vis the simple diphosphine ligand (*Z*)-$Ph_2PCH{=}CHPPh_2$ towards P–C bond cleavage is consistent with the assertions put forth by Garrou [17] on the enhanced degradation reactivity of phosphine bearing electron-withdrawing substituents and with our observations on the facile formation of phosphido-bridged clusters from bma-substituted clusters [1–5]. Attempts to spectroscopically detect $PhCCo_2MoCp(CO)_6$(bma) during our reactions by IR spectroscopy were not successful. This observation requires that the ensuing P–C bond cleavage and reductive coupling between the maleic anhydride ring and the benzylidyne ligand must occur more rapidly relative to the formation of $PhCCo_2MoCp(CO)_6$(bma). Independent thermolysis of pure **3** in refluxing CH_2Cl_2 gives cluster **4**, thus confirming that **3** is a precursor to **4**. The top portion of Scheme 2 outlines the course of the substitution reaction between $PhCCo_2MoCp(CO)_8$ and bma.

The IR spectrum for **3** exhibits terminal ν(CO) bands at 2052 (s), 2034 (vs), 2016 (m), 1998 (m) cm^{-1}, along with two lower frequency carbonyl stretches at 1800 and 1743 cm^{-1} that were initially assumed to represent the vibrationally coupled C=O groups of the maleic anhydride ring [18]. However, closer inspection of the higher energy C=O band showed atypical broadening and asymmetry and suggested that this carbonyl band was actually composed of two, overlapping carbonyls from a bridging carbonyl group associated with the cluster and the expected symmetric ν(CO) stretch from the maleic anhydride moiety. The low-temperature ^{13}C NMR spectrum of a sample of ^{13}CO-enriched **3** displayed four terminal Co–CO resonances at δ 193.45, 195.45, 201.81, 202.82 and one bridging CO resonance at δ 241.52 [19], while the ^{31}P NMR spec-

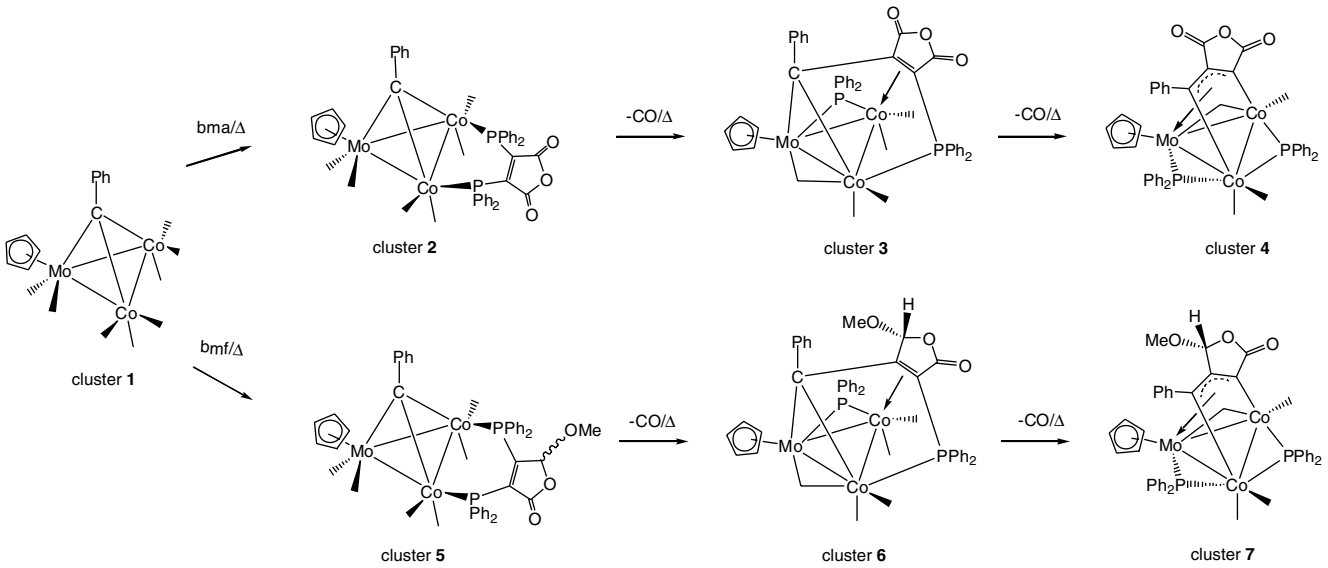

Scheme 2.

trum revealed the presence of two singlets at δ 179.59 and 21.29 that are readily ascribed to a bridging phosphido group and phosphine moiety, respectively [20].

The molecular structure for **3**, as the ether solvate, was established by X-ray crystallography. The ORTEP diagram of **3** is depicted in Fig. 1. This cluster contains 48-valence electrons and possesses a highly asymmetric triangular Co_2Mo core based on the Co(1)–Co(2), Co(1)–Mo, and Co(2)–Mo bond distances of 2.643(6), 2.699(5), and 2.929(4) Å, respectively. While the former two distances exhibit bond lengths that parallel those distances found in other Co_2Mo tetrahedrane clusters [6,21], the latter Co(2)–Mo vector is elongated by ca. 0.15 Å relative to those Co–Mo bond distances reported in Co_2Mo tetrahedrane clusters and other Co/Mo polynuclear motifs [21,22]. The six-electron ligand μ_2,η^2,η^1-C(Ph)C=C(PPh_2)C(O)OC(O), which results from the formal cleavage of a Ph_2P–C(maleic anhydride) bond and reductive coupling of the resulting σ-bound Co–C(maleic anhydride) moiety with the benzylidyne capping ligand, caps one of the Co_2Mo faces in a fashion analogous to that of the tricobalt cluster $Co_3(CO)_6[\mu_2,\eta^2,\eta^1$-C(Ph)C=C($PPh_2$)C(O)OC(O)](μ-$PPh_2$) [1]. The bridging phosphido moiety that spans the Mo–Co(2) vector displays bond distances of 2.354(8) Å [Mo–P(2)] and 2.272(7) Å [Co(2)–P(2)] and is situated below the metallic plane opposite the face-capping μ_2,η^2,η^1-C(Ph)C=C(PPh_2)C(O)-OC(O) ligand. Of the five carbonyl groups in **3**, the Mo–C(1)–O(1) and Co(1)–C(1)–O(1) linkages are clearly bridging and exhibit angles of 168(2)° and 113(2)°, respectively [23]. The benzylidene moiety that bridges the Co(1)–Mo vector exhibits Co(1)–C(16) [2.05(2) Å] and Mo–C(16) [2.12(2) Å] bond distances that are unexceptional to those distances found in Co_xMo_n clusters containing benzylidyne and benzylidene ligands [6,21,24].

Cluster **4** was characterized in solution by IR and NMR spectroscopies and X-ray diffraction analysis. The principal IR spectroscopic features include three terminal carbonyl bands at 2056 (vs), 2024 (m), and 1948 (s) cm^{-1}, in addition to carbonyl stretching bands at 1815 (m) and 1756 (m) assignable to the maleic anhydride residue and one lone cluster-bound μ_2-CO band at 1785 (s) cm^{-1}. The shift to higher energy for the kinematically coupled anhydride C=O groups (ca. 15 cm^{-1}) is consistent with the activation and release of the second phosphine moiety, as this would yield a less electron-rich anhydride ring. The ^{31}P NMR spectrum of **4** shows two doublets at δ 209.04 and 251.93 ($J_{P-P} = 48$ Hz) for the two phosphido ligands. Four distinct CO resonances were recorded in the low-temperature ^{13}C NMR spectrum of cluster **4**, all of which integrated for a single CO group. The chemical shifts found for the terminal CO groups (δ 191.73, 200.51, and 207.94) and the one bridging CO group (δ 250.52) are in keeping with the structure of **4** and the ^{13}C NMR assignments in related cluster systems [8a,21a,25].

The ORTEP diagram of **4** shown in Fig. 1 establishes the presence of the second phosphido moiety in going from **3** → **4**. This represents the first example involving the double cleavage of the Ph_2P–C(maleic anhydride) bonds from a cluster-coordinated bma ligand. Cluster **4** contains 48-valence electrons and exhibits a near equilateral Co_2Mo triangle, where the metal–metal bond distances range from 2.627(3) Å[Co(1)–Mo] to 2.748(3) Å[Co(2)–Mo] and display a mean value of 2.680 Å. The two phosphido groups are bound to the Co(1)–Co(2) and Co(1)–Mo vectors in a highly asymmetric fashion but within acceptable ranges found for other μ_2-PPh_2 moieties that are tethered to Co–Co and Co–Mo bonds [1–4,26,27]. The presence of the face-capping, five-electron donor ligand η^3,η^1,η^1-

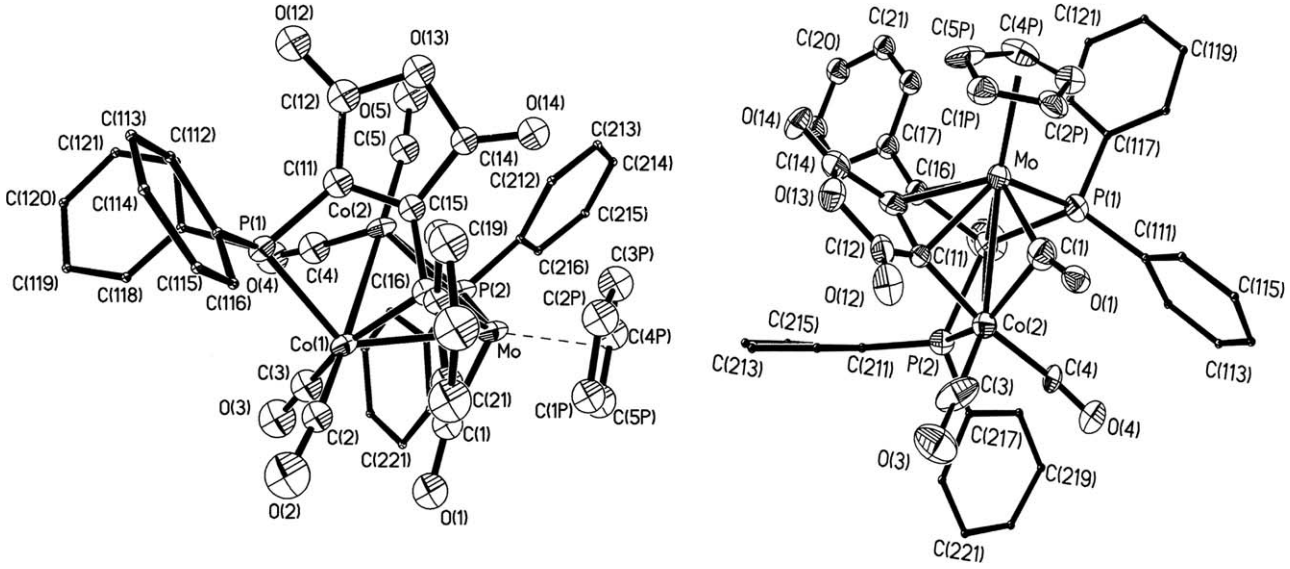

Fig. 1. ORTEP diagrams of $Co_2MoCp(CO)_4$(μ-CO)[μ_2,η^2,η^1-C(Ph)C=C(PPh_2)C(O)OC(O)](μ-PPh_2) (**3**; left) and $Co_2MoCp(CO)_3$(μ-CO)[η^3,η^1,η^1-C(Ph)C=CC(O)OC(O)](μ-PPh_2)$_2$ (**4**; right) showing the thermal ellipsoids at the 30% probability level.

C(Ph)C=CC(O)OC(O) is of interest because it functions as a 1e- σ donor (η^1) to each cobalt center and as a delocalized 3e- π-allyl ligand (η^3) to the molybdenum center. This σ,σ,π bonding of the ancillary ligand C(Ph)C=CC(O)-OC(O) to the Co_2Mo cluster face was not expected given the ligation of the Mo–Co(1) bond by the C(16) atom in cluster **3** through a normal benzylidene or carbene-type interaction involving two σ M–C bonds. Support for the η^3-allylic π bonding of the C(11)–C(15)–C(16) atoms to the Mo center is seen in the two sets of distinctly different metal–C bond distances for the attachment of the C(Ph)C=CC(O)OC(O) ligand to the triangular Co_2Mo face. Here the traditional Co–C σ bonds defined by the Co(2)–C(11) [1.93(2) Å] and Co(1)–C(16) [1.92(2) Å] vectors are clearly shorter than the allylic system composed of the Mo–C(11) [2.22(2) Å], Mo–C(15) [2.31(2) Å] and Mo–C(16) [2.44(2) Å] bonds [28–30]. Finally, the bridging C(1)O(1) group that spans the Mo–Co(2) bond exhibits bond distances [Mo–C(1) = 1.98(2) Å; Co(2)–C(1) = 2.12(2) Å] and angles [Mo–C(1)–O(1) = 156(1)°; Co(2)–C(1)–O(1) = 119(1)°] that confirms that the solid-state and solution structures adopted by cluster **4** are not significantly different.

3.2. Synthesis, spectroscopic data, and X-ray diffractions structures for $Co_2MoCp(CO)_5[\mu_2,\eta^2,\eta^1$-C(Ph)C=C(PPh$_2$)C(O)OCH(OMe)](μ-PPh$_2$) (**6**) and $Co_2MoCp(CO)_4[\eta^3,\eta^1,\eta^1$-C(Ph)C=CC(O)OCH(OMe)](μ-PPh$_2$)$_2$ (**7**)

The reaction between $PhCCo_2MoCp(CO)_8$ with the chiral ligand bmf proceeds similarly as that described for bma. Accordingly, we will only present the highlights of these reactions. Unlike the reaction between cluster **1** and the symmetric bma ligand, the coordination of the bmf ligand to **1** raises interesting questions concerning the regioselectivity for the Ph_2P–C(furanone) bond cleavage and the diastereoselectivity that accompanies the activation of the ancillary diphosphine ligand. Thermolysis of **1** with bmf in refluxing CH_2Cl_2 produces the new cluster compounds $Co_2MoCp(CO)_5[\mu_2,\eta^2,\eta^1$-C(Ph)C=C(PPh$_2$)C(O)OCH(OMe)](μ-PPh$_2$) (**6**) and $Co_2MoCp(CO)_4[\eta^3,\eta^1,\eta^1$-C(Ph)C-CC(O)OCH(OMe)](μ-PPh$_2$)$_2$ (**7**), presumably through the bmf-substituted cluster $PhCCo_2MoCp(CO)_6$(bmf). The bottom portion of Scheme 2 illustrates the course of these reactions. Both **6** and **7** were isolated by chromatographic separation and characterized by solution, elemental, and X-ray diffraction analyses.

The ^{1}H NMR spectrum of **6** displays singlet resonances for the methine hydrogen and the OMe group at C-5 of the furanone ring (δ 5.68 and 2.81, respectively). These data indicate that cluster **6** is produced as a single diastereomer. The ORTEP diagram of **6** shown in Fig. 2 confirms this contention. Here the two stereocenters are defined by the C-141 atom of the furanone ring and the original benzylidyne carbon atom in **1** that is transformed into a chiral center following the reductive coupling of the benzylidyne moiety with the furanone alkenyl carbon C-15. This latter reaction is triggered by the scission of the Ph_2P–C(furanone) bond. The phosphido moiety is bound across the Mo–Co(2) bond in **6**, which in turn allows us to trace the origin of this μ-PPh$_2$ ligand to the original phosphine moiety that was conjugated to the carbonyl group of the bmf ligand in the putative cluster $PhCCo_2MoCp(CO)_6$(bmf). The solution NMR and structural data support the regioselectivity found in the P–C bond cleavage reaction leading to **6**. Here the less basic phosphine group (i.e., the one in conjugation with the furanone carbonyl) is expected to participate more readily in the P–C bond activation either by a dissociation from or a slippage away from the metal center

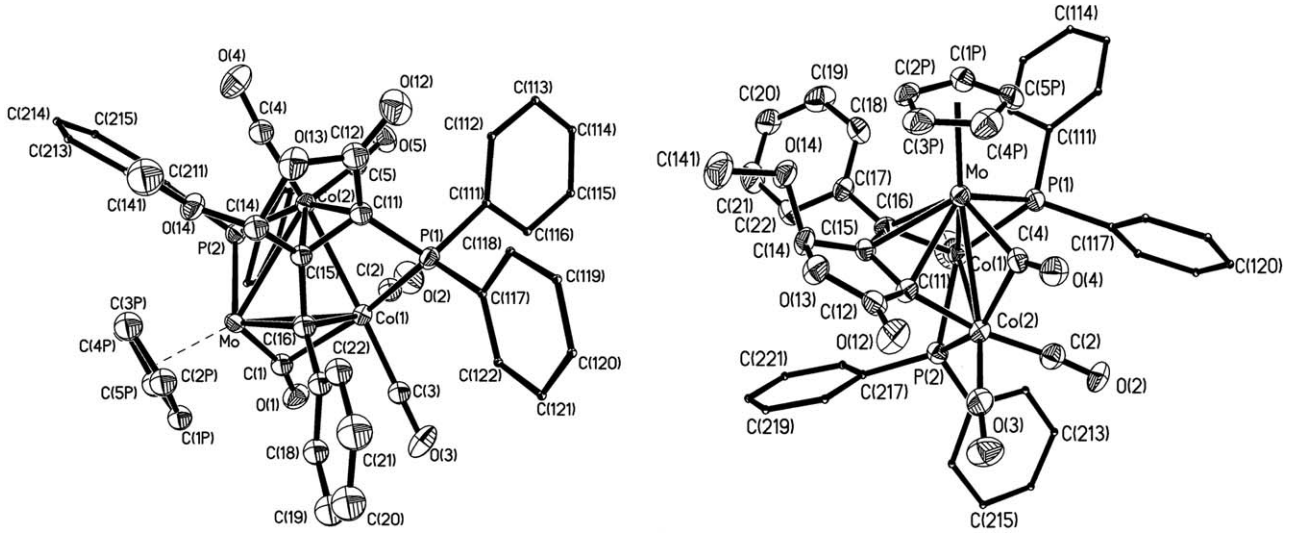

Fig. 2. ORTEP diagrams of $Co_2MoCp(CO)_4$(μ-CO)[μ_2,η^2,η^1-C(Ph)C=C(PPh$_2$)C(O)OCH(OMe)](μ-PPh$_2$) (**6**; left) and $Co_2MoCp(CO)_3$(μ-CO)[η^3,η^1,η^1-C(Ph)C=CC(O)OCH(OMe)](μ-PPh$_2$)$_2$ (**7**; right) showing the thermal ellipsoids at the 30% probability level.

in comparison to the other more basic and strongly bound PPh_2 moiety. In keeping with the premise, we have confirmed the preferential dissociation of the less basic phosphine moiety in the coordinated bmf ligand in the related tetrahedrane cluster $HCCo_2NiCp(CO)_4$(bmf) [4]. The 6e-donor ligand μ_2,η^2,η^1-C(H)C=C(PPh_2)C(O)OCH(OMe) in **6** caps the Co_2Mo face in a manner identical to that exhibited by **3** and the bma-activated ligand in $Co_3(CO)_6[\mu_2,\eta^2,\eta^1$-C(Ph)C=C($PPh_2$)C(O)OC(O)]($\mu$-$PPh_2$) [1]. It is our belief that the observed diastereoselectivity that accompanies the formation of **6** may be traced to the methoxy group that is attached to furanone C(14) atom and its interactions with neighboring groups. Here the methoxy group is seen to adopt a proximal or syn disposition with respect the phosphido moiety that spans the Mo–Co(2) vector and a distal or anti orientation to the nearby phenyl group defined by the C(17)–C(22) atoms. It is the latter phenyl group that is instrumental in controlling the stereochemistry in **6**, as the alternative diastereomer having syn methoxy and phenyl [C(17)–C(22) atoms] substituents would place these two groups in close proximity, leading to unfavorable van der Waals interactions.

The pertinent spectroscopic data for **7** include two low-field ^{31}P resonances at δ 213.33 and 251.54 and one set of furanone hydrogens for the methine and methoxy groups at δ 5.82 and 2.66, respectively, in the ^1H NMR spectrum. The ^1H NMR data support the presence of only one diastereomer for **7** in solution, as was subsequently verified by X-ray crystallography. The ORTEP diagram of **7** that is depicted in Fig. 2 clearly confirms the cleavage of the remaining P–C(furanone) bond in the precursor cluster **6** [31]. The two phosphido moieties serve as bridging ligands and span the Mo–Co(1) and Co(1)–Co(2) vectors. Cluster **7** contains 48-valence electrons and is identical to cluster **5** in terms of the observed structural data. The three-carbon atoms C(11)–C(15)–C(16) that comprise the allylic moiety are π-bound to the Mo atom in a conventional η^3 fashion. The one major point of difference between **7** and its bma-derived analogue **5** concerns the ancillary methoxy group and its stereochemical disposition relative to the metallic frame and other ligands. The methoxy group is oriented over the carbonyl-bridged Mo–Co(2) bond and is skewed slightly towards the Mo center. Adoption of this conformation allows the MeO group to avoid close contacts and extenuating destablization with the nearby phenyl group comprised by the C(16)–C(22) atoms and the phosphido group that bridges the Mo–Co(1) bond.

3.3. Electrochemical and MO data

The cyclic voltammetric properties of clusters **3**, **4**, **6**, and **7** were next investigated due to the rich electrochemistry displayed by the parent cluster $PhCCo_2MoCp(CO)_8$[32] and the diverse redox chemistry exhibited by bma- and bmf-substituted di- and polynuclear compounds prepared by us [33]. The CV data of each cluster were recorded at platinum electrodes in CH_2Cl_2 solvent containing 0.2 M TBAP as the supporting electrolyte. Since the phosphido clusters **3** and **6** and the bis(phosphido) clusters **4** and **7** are qualitatively similar, we will only present the CV data for the bma-derived clusters **3** and **4**. Fig. 3 shows the CV for **3** recorded at room temperature and at a scan rate of 100 mV/s. The three diffusion-controlled processes observed at $E_{1/2} = 0.66$, -0.77, and -1.41 V are assigned to the 0/+1, 0/−1, −1/−2 redox couples [34]. The former two redox couples are fully reversible and display a peak-to-peak separation of ca. 85 mV, which is slightly larger than the Nernstian value of 59 mV but whose value is similar to that found for internally added $Cp^*_2Fe/Cp^*_2Fe^+$. This behavior is indicative of internal solution resistance due to the CH_2Cl_2 solvent and not a slow electron-transfer process (i.e., k_{het} low). The −1/−2 redox couple exhibits a ΔE_p value of 170 mV that is consistent with either a low k_{het} value or a structural reorganization. These reduction data show a close parallel to those dc and differential pulse polarographic data reported for the parent cluster **1**, whose LUMO was ascribed to an antibonding σ^* orbital involving the metallic framework [32,35]. Extended Hückel MO calculations on the model cluster $Co_2MoCp(CO)_5[\mu_2,\eta^2,\eta^1$-C(H)C=C($PH_2$)C(O)OC(O)]($\mu$-$PH_2$) revealed a metal-based LUMO at −10.19 eV having a_2 symmetry in excellent agreement with the EPR data obtained from related tetrahedrane clusters and the MO calculations [32,35–37]. The HOMO for $Co_2MoCp(CO)_5[\mu_2,\eta^2,\eta^1$-C(H)C=C($PH_2$)-C(O)OC(O)]($\mu$-$PH_2$) occurs at −11.20 eV and is best viewed as a metal-based orbital that is composed largely of a hybridized d_{xz} molybdenum orbital, with added π^* interactions between the Mo center and the bridging benzylidene carbon and the Mo–CO group.

The bis(phosphido)-bridged cluster $Co_2MoCp(CO)_4[\eta^3,\eta^1,\eta^1$-C(Ph)C=CC(O)OC(O)]($\mu$-$PPh_2$)$_2$ was examined by cyclic voltammetry in a manner identical to that reported for **3**. Cluster **4** exhibits a reversible one-electron oxidation at $E_{1/2} = 0.52$ V that is assigned to the 0/+1 redox couple. Whereas the second P–C bond activation in going from **3** → **4** does not negatively affect the oxidation couple, the

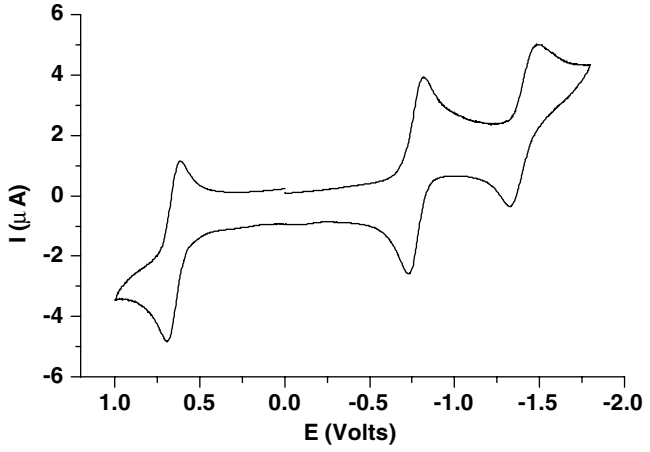

Fig. 3. Room temperature cathodic scan cyclic voltammogram for cluster **3** ca. 10^{-3} M in CH_2Cl_2 containing 0.2 M TBAP at 100 mV/s.

kinetic stability of the 0/−1 redox couple is greatly diminished. Here a quasi-reversible one-electron wave was observed at $E_{1/2} = -1.03$ V at a scan rate of 100 mV/s. The current ratio (I_p^a/I_p^c) of ca. 0.5 and the presence of additional anodic waves at $E_p^a = -0.57$ and -0.28 V all indicate that the radical anion of $\mathbf{4}^{\cdot-}$ is not stable, leading to partial decomposition on the CV time scale. Increasing the scan rate up to 1.0 V/s and dropping the temperature down to 0 °C did not improve the CV behavior of **4**.

4. Conclusions

Thermolysis of the mixed-metal cluster $PhCCo_2MoCp(CO)_8$ with the diphosphine ligands bma and bmf in CH_2Cl_2 leads to facile and sequential P–C bond cleavage and formation of the new clusters $Co_2MoCp(CO)_5[\mu_2,\eta^2,\eta^1\text{-}C(Ph)C{=}C(PPh_2)C(O)OC(O)](\mu\text{-}PPh_2)$ (**3**) and $Co_2MoCp(CO)_4[\eta^3,\eta^1,\eta^1\text{-}C(Ph)C{=}CC(O)OC(O)](\mu\text{-}PPh_2)_2$ (**4**) from bma and $Co_2MoCp(CO)_5[\mu_2,\eta^2,\eta^1\text{-}C(Ph)C{=}C(PPh_2)C(O)OCH(OMe)](\mu\text{-}PPh_2)$ (**6**) and $Co_2MoCp(CO)_4[\eta^3,\eta^1,\eta^1\text{-}C(Ph)C{=}CC(O)OCH(OMe)](\mu\text{-}PPh_2)_2$ (**7**) from bmf. The molecular structures of all four products have been established by X-ray crystallography, with excellent agreement found between the solid-state and solution structures. In the case of the chiral bmf ligand, high regio- and diastereoselectivity are observed during the formation of cluster **6** and its transformation to cluster **7**. Future bma and bmf substitution studies on Co_2Mo clusters that contain different capping alkylidyne ligands are planned, and the ability of clusters **4** and **7** to serve as allyl-transfer agents in synthetic organic reactions will be investigated by us.

5. Supporting information

Crystallographic data for the structural analysis have been deposited with the Cambridge Crystallographic Data Center, CCDC No. 276391 for **3**; 276392 for **4**; 274194 for **6**; and 274193 for **7**. Copies of these data may be obtained free of charge from the Director, CCDC, 12 Union Road, Cambridge, CB2 1EZ UK [fax: +44(1223)336 033; email: deposit@ccdc.ac.uk or http://www:ccdc.cam.ac.uk].

Acknowledgment

Financial support from the Robert A. Welch Foundation (B-1093-MGR) is appreciated.

References

[1] K. Yang, J.M. Smith, S.G. Bott, M.G. Richmond, Organometallics 12 (1993) 4779.
[2] S.G. Bott, K. Yang, K.A. Talafuse, M.G. Richmond, Organometallics 22 (2003) 1383.
[3] S.G. Bott, K. Yang, M.G. Richmond, J. Organomet. Chem. 690 (2005) 3067.
[4] S.G. Bott, K. Yang, M.G. Richmond, J. Organomet. Chem. 691 (2006) 20.
[5] Y. Yang, S.G. Bott, M.G. Richmond, J. Organomet. Chem. 454 (1993) 273.
[6] S.G. Bott, K. Yang, S.-H. Huang, M.G. Richmond, J. Chem. Crystallogr. 34 (2004) 883.
[7] For a report dealing with the regioselective phosphine attack on a coordinated alkyne by the bmf ligand, see: K. Yang, S.G. Bott, M.G. Richmond, Organometallics 14 (1995) 4977.
[8] (a) For NMR studies dealing with ligand fluxionality in RCCo2-$MoCp(CO)_{8-n}P_n$ clusters, see: K.A. Sutin, J.W. Kolis, M. Mlekuz, P. Bougeard, B.G. Sayer, M.A. Quilliam, R. Faggiani, C.J.L. Lock, M.J. McGlinchey, G. Jaouen, Organometallics 6 (1987) 439;
(b) D.T. Clark, K.A. Sutin, M.J. McGlinchey, Organometallics 8 (1989) 155.
[9] (a) R. Blumhofer, K. Fischer, H. Vahrenkamp, Chem. Ber. 119 (1986) 194;
(b) H. Beurich, R. Blumhofer, H. Vahrenkamp, Chem. Ber. 115 (1982) 2409.
[10] D.T. Mowry, Am. Chem. Soc. 72 (1950) 2535.
[11] (a) D. Fenske, H.J. Becher, Chem. Ber. 108 (1975) 2115;
Chem. Ber. 107 (1974) 117;
(b) D. Fenske, Chem. Ber. 112 (1979) 363.
[12] D.F. Shriver, The Manipulation of Air-Sensitive Compounds, McGraw-Hill, New York, 1969.
[13] (a) R. Hoffmann, W.N. Libscomb, J. Chem. Phys. 36 (1962) 2179;
(b) R. Hoffmann, J. Chem. Phys. 39 (1963) 1397.
[14] C. Mealli, D.M. Proserpio, J. Chem. Ed. 67 (1990) 399.
[15] R.C. Weast (Ed.), Handbook of Chemistry and Physics, 56 ed., CRC Press, Cleveland, OH, 1975.
[16] M.F. Ryan, D.E. Richardson, D.L. Lichtenberger, N.E. Gruhn, Organometallics 13 (1994) 1190.
[17] (a) P.E. Garrou, Chem. Rev. 85 (1985) 171;
(b) R.A. Dubois, P.E. Garrou, Organometallics 5 (1986) 466.
[18] N.B. Colthup, L.H. Daly, S.E. Wiberley, Introduction to Infrared and Raman Spectroscopy, 3rd ed., Academic Press, New York, 1990.
[19] The ancillary CO ligands in the phosphido-bridged clusters **3**, **4**, **6**, and **7** show no evidence for intramolecular scrambling at room temperature. The ^{13}C NMR data were recorded at low temperature to minimize the ^{59}Co quadrupolar coupling with the attached CO ligand. See: M. Schwartz, M.G. Richmond, A.F.T. Chen, G.E. Martin, J.K. Kochi, Inorg. Chem. 27 (1988) 4698.
[20] (a) P.E. Garrou, Chem. Rev. 81 (1981) 229;
(b) A.J. Carty, S.A. MacLaughlin, D. Nucciarone, in: J.G. Verkade, L.D. Quin (Eds.), Phosphorus-31 NMR Spectroscopy in Stereochemical Analysis: Organic Compounds and Metal Complexes, VCH Publishers, New York, 1987 (Chapter 16).
[21] (a) K.A. Sutin, L. Li, C.S. Frampton, B.G. Sayer, M.J. McGlinchey, Organometallics 10 (1991) 2362;
(b) D.N. Duffy, M.M. Kassis, A.D. Rae, J. Organomet. Chem. 460 (1993) 97;
(c) H. Shimomura, X. Lei, M. Shang, T.P. Fehlner, Organometallics 16 (1997) 5302;
(d) E.N. Jacobsen, R.G. Bergman, J. Am. Chem. Soc. 107 (1985) 2023;
(e) H. Adams, L.V.Y. Guio, M.J. Morris, S.E. Spey, J. Chem. Soc., Dalton Trans. (2002) 2907;
(f) H.-P. Wu, Y.-Q. Yin, X.-Y. Huang, Inorg. Chim. Acta 255 (1997) 167;
(g) M.I. Bruce, J.-F. Halet, S. Kahlal, P.J. Low, B.W. Skelton, A.H. White, J. Organomet. Chem. 578 (1999) 155.
[22] (a) E.P. Kyba, M.C. Kerby, R.P. Kashyap, J.A. Mountzouris, R.E. Davis, Organometallics 8 (1989) 852;
(b) O.J. Curnow, J.W. Kampf, M.D. Curtis, Organometallics 10 (1991) 2546;
(c) U. Riaz, M.D. Curtis, A. Rheingold, B.S. Haggerty, Organometallics 9 (1990) 2647;
(d) C.P. Gibson, L.F. Dahl, Organometallics 7 (1988) 543;
(e) H.-T. Schacht, H. Vahrenkamp, Chem. Ber. 122 (1989) 2239.
[23] C.P. Horwitz, D.F. Shriver, Adv. Organomet. Chem. 23 (1984) 219.

[24] (a) R.D. Adams, J.A. Belinski, Organometallics 10 (1991) 2114;
(b) H. Beurich, H. Vahrenkamp, Chem. Ber. 115 (1982) 2385;
(c) H. Adams, L.J. Gill, M.J. Morris, J. Chem. Soc., Dalton Trans. (1996) 3909;
(d) Y. Yin, H. Sun, D. Jin, Y. Zhu, J. Organomet. Chem. 439 (1992) 45;
(e) H.-P. Wu, Y.-Q. Yin, X.-Y. Huang, K.-B. Yu, J. Organomet. Chem. 498 (1995) 119.
[25] M.G. Richmond, J.K. Kochi, Inorg. Chem. 25 (1986) 1334.
[26] (a) A.D. Harley, R.R. Whittle, G.L. Geoffroy, Organometallics 2 (1983) 60;
(b) S. Onaka, H. Muto, Y. Katsukawa, S. Takagi, J. Organomet. Chem. 543 (1997) 241.
[27] (a) J.D. King, M.J. Mays, G.E. Pateman, P.R. Raithby, M.A. Rennie, G.A. Solan, N. Choi, G. Conole, M. McPartlin, J. Chem. Soc., Dalton Trans. (1999) 4447;
(b) M.J. Mays, P.R. Raithby, K. Sarveswaran, G.A. Solan, J. Chem. Soc., Dalton Trans. (2002) 1671;
(c) A. Martin, M.J. Mays, P.R. Raithby, G.A. Solan, J. Chem. Soc., Dalton Trans. (1993) 1431;
(d) M.R. Bradford, N.G. Connelly, N.C. Harrison, J.C. Jeffery, Organometallics 8 (1989) 1829.
[28] (a) For examples of mixed-metal Co/Mo clusters that display comparable Co–C sigma-bond distances, see: J. Zhang, X.-N. Chen, Y.-Q. Yin, X.-Y. Huang, J. Organomet. Chem. 579 (1999) 304;
(b) M.J. Chetcuti, P.E. Fanwick, J.C. Gordon, Inorg. Chem. 30 (1991) 4710;
(c) H. Adams, N.A. Bailey, L.J. Gill, M.J. Morris, F.A. Wildgoose, J. Chem. Soc., Dalton Trans. (1996) 1437.
[29] (a) For examples of sundry mixed-metal clusters that contain a Mo-(η^3-allyl) moiety and possess similar Mo–C π-bond distances to those in cluster **4**, see: P. Mathur, M.O. Ahmed, J.K. Kaldis, M.J. McGlinchey, J. Chem. Soc., Dalton Trans. (2002) 619;
(b) C.M. Hay, A.D. Horton, M.J. Mays, P.R. Raithby, Polyhedron 7 (1988) 987;
(c) R.D. Adams, J.E. Babin, M. Tasi, Organometallics 6 (1987) 2247;
(d) R.D. Adams, J.E. Babin, M. Tasi, J.-G. Wang, Organometallics 7 (1988) 755.
[30] (a) For structural reports of related 1,3-dimetalloallyl derivatives, see: M.R. Churchill, L.A. Buttrey, J.B. Keister, J.W. Ziller, T.S. Janik, W.S. Striejewske, Organometallics 9 (1990) 766;
(b) K.M. Rao, R.J. Angelici, V.G. Young Jr., Inorg. Chim. Acta 198–200 (1992) 211;
(c) C.-G. Xia, S.G. Bott, M.G. Richmond, J. Chem. Crystallogr. 33 (2003) 681;
(d) M.-T. Kuo, D.-K. Hwang, C.-S. Liu, Y. Chi, S.-M. Peng, G.-H. Lee, Organometallics 13 (1994) 2142.
[31] Independent thermolysis experiments starting with isolated **6** did indeed furnish **7** in keeping with our thinking concerning the stepwise or sequential nature of these double P–C bond cleavage reactions.
[32] P.N. Lindsay, B.M. Peake, B.H. Robinson, J. Simpson, U. Honrath, H. Vahrenkamp, A.M. Bond, Organometallics 3 (1984) 413.
[33] (a) K. Yang, S.G. Bott, M.G. Richmond, J. Organomet. Chem. 516 (1996) 65;
(b) K. Yang, S.G. Bott, M.G. Richmond, J. Organomet. Chem. 689 (2004) 791;
(c) K. Yang, J.A. Martin, S.G. Bott, M.G. Richmond, Organometallics 15 (1996) 2227;
(d) C.-G. Xia, K. Yang, S.G. Bott, M.G. Richmond, Organometallics 15 (1996) 4480;
(e) N.W. Duffy, R.R. Nelson, M.G. Richmond, A.L. Rieger, P.H. Rieger, B.H. Robinson, D.R. Tyler, J.C. Wang, K. Yang, Inorg. Chem. 37 (1998) 4849;
(f) K. Yang, S.G. Bott, M.G. Richmond, J. Chem. Crystallogr. 35 (2005) 719.
[34] (a) For discussions and details related to the criteria used to assess electrochemical reversibility (i.e., linear plots of I_p versus $v^{1/2}$; unity current ratios, ΔE_p values), see: P.H. Rieger, Electrochemistry, Chapman & Hall, New York, 1994;
(b) A.J. Bard, L.F. Faulkner, Electrochemical Methods, Wiley, New York, 1980.
[35] B.E.R. Schilling, R. Hoffmann, J. Am. Chem. Soc. 101 (1979) 3456.
[36] (a) D.L. Stevenson, C.H. Wei, L.F. Dahl, J. Am. Chem. Soc. 93 (1971) 6027;
(b) T.W. Matheson, B.M. Peake, B.H. Robinson, J. Simpson, D.J. Watson, J. Chem. Soc., Chem. Commun. (1973) 894;
(c) B.M. Peake, B.H. Robinson, J. Simpson, D.J. Watson, Inorg. Chem. 16 (1977) 405;
(d) H. Beurich, T. Madach, F. Richter, H. Vahrenkamp, Angew. Chem. 91 (1979) 751;
(e) B.M. Peake, P.H. Rieger, B.H. Robinson, J. Simpson, Inorg. Chem. 18 (1979) 1000.
[37] (a) P.T. Chesky, M.B. Hall, Inorg. Chem. 20 (1981) 4419;
(b) R.L. DeKock, P. Deshmukh, T.K. Dutta, T.P. Fehlner, C.E. Housecroft, J. L.-S. Hwang, Organometallics 2 (1983) 1108.